Optical and Quantum Electronics (2020) 52:335
https://doi.org/10.1007/s11082-020-02448-9

Impact of film thickness on optical properties and optoelectrical parameters of novel $CuGaGeSe_4$ thin films synthesized by electron beam deposition

Ahmed Saeed Hassanien[1,2] · Hatem R. Alamri[3] · I. M. El Radaf[4,5]

Received: 14 January 2020 / Accepted: 17 June 2020 / Published online: 28 June 2020

Abstract
The authors in this article present the synthesis of good quality $CuGaGeSe_4$ thin films of different thicknesses using electron beam deposition on well pre-cleaned glass substrates. X-ray diffraction patterns displayed the amorphous nature of as-prepared $CuGaGeSe_4$ thin films. In addition, the elemental compositional analysis of these films was examined by the energy-dispersive X-ray spectroscopy technique, which showed that there is good matching between the selected and detected percentages. Transmittance and reflectance spectra of these $CuGaGeSe_4$ samples were measured to experimentally determine the absorption coefficient and some related optical parameters. Optical band-gap energy values of samples were determined via Tauc's Plots; they are arisen owing to the indirect allowed transition. They are decreased from 1.43 to 1.29 eV by increasing the film thickness from 250 to 445 nm. The skin depth, absorption index, and refractive index of $CuGaGeSe_4$ thin films were also obtained and extensively studied. As well as, some optoelectrical parameters of these investigated films were discussed, like optical resistivity, optical mobility, optical conductivity, the lattice dielectric constant, and the ratio of the charge carrier concentrations to the effective mass (N_{opt}/m^*). Along with, some nonlinear optical parameters of $CuGaGeSe_4$ films were studied employing Miller's formulas. The values of the dispersion energy, static refractive index, the static dielectric constant, the oscillator strength and others increase, while the oscillator energy and the relaxation time decrease as the film thickness increased. The obtained results showed that these $CuGaGeSe_4$ film samples can be successfully used as absorption layers in thin-film solar cells.

Keywords $CuGaGeSe_4$ thin films · Electron beam deposition · Optical conductivity · Optical constants · Third-order nonlinear optical susceptibility

✉ I. M. El Radaf
elradaf11b@gmail.com; i.radaf@qu.edu.sa

Extended author information available on the last page of the article

1 Introduction

Recently, the quaternary chalcogenide glasses, ChG based on the copper element have attracted high interest owing to their distinguished and interesting optical, optoelectronic, and electrical properties. These ChG semiconducting compounds have high thermal stability and high absorption coefficient (Hassanien et al. 2020a, b; Aldakov et al. 2013; Chen et al. 2009, 2010). These unique properties make these quaternary chalcogenides suitable for different applications like the optical memory devices, absorber layer for solar cells, IR sensors, and photodetectors (Hassanien and Akl 2018c; Benchikri et al. 2012; Liu et al. 2009; Ramasamy et al. 2016).

In the past, the scientists and researchers were concentrated on the quaternary $CuInGaSe_2$, CIGS thin films as a good absorber layer for thin-film solar cells (Shi et al. 2011). But the high costs of the fabrication of these CIGS thin films make the scientists and researchers try to find a new and low-cost family of such quaternary chalcogenide glasses, QChG. This QChG new family is based on the formula A_2BCX_4 where A is (Cu or Ag), B is (Zn or Mn or Cd), C is (Sn or Ge), and X is (S or Se) (Hassanien and El Radaf 2020). It worth to mention that this new family called kesterite materials (Schäfer and Nitsche 1974; El Radaf et al. 2020).

These QChG-semiconducting materials can be fabricated by many different techniques; like spray pyrolysis (El Radaf et al. 2019a, b), dip coating (Ziti et al. 2019), thermal evaporation (Shi et al. 2012), electrodeposition (Scragg et al. 2009) and chemical bath deposition (Fouad et al. 2018). Among all these materials, the films of Cu_2ZnSnS_4 compositions have promising optical and electrical properties (Schurr et al. 2009). In previous literature, Cu_2ZnSnS_4 thin films have been found to have very good photoelectric properties. So, they are considered as desirable materials used as important absorption layers in thin-film solar cells. Moreover, owing to their earth availability, stability, inexpensive preparation, non-toxicity, and easy to prepare (Ramasamy et al. 2012).

Furthermore, there is also another promising quaternary family, based on the structure of $CuABX_4$, where B is (In or Ga), C is (Sn or Ge) and X is (S or Se) (Zamani et al. 2014). This family has also good optical and electrical properties and can be used as a good absorber for thin-film solar cells. Consequently, it become for researchers three compositions or groups; they are CuInGeSe4, CuInGeS4, and CuGaGeSe4, used to fabricate absorbing thin-film solar cells. In a previous research work on the CuInGeSe4 thin films (Hameed et al. 2018), these films have displayed that they are very good absorber layers. At the same time, they produce CuInGeSe4/n-Si heterojunction with a solar efficiency of 2.83%.

The aim of the present research is to prepare the novel $CuGaGeSe_4$ thin films using the electron beam deposition technique, for the first time. The authors have tried to prepare these novel film samples and to have good quality and have optical and electrical properties similar to $CuInGeSe_4$ thin films. Then, authors have studied and discussed the linear, nonlinear optical characteristics and some optoelectrical parameters of these film samples of different thicknesses.

As our knowledge, there is no article reported the fabrication and study of the optical characterizations of the $CuGaGeSe_4$ thin films. Therefore, the authors found it difficult to refer to any previously published references, but they substituted this by comparing their obtained results with similar researches which their samples are consistent with the present samples of this work.

2 Experimental details

In this study, copper gallium germanium selenide ($CuGaGeSe_4$) bulk compositions were prepared via direct melting of a mixture of pure elements (Cu, Ga, Ge, and Se) with purity 99.999% each. The atomic proportions of the constituents' elements were adjusted to be (1:1:1:4). Then the mixture of elements has been sealed in a silica tube under vacuum of 10^{-3} Pa. A rocking electric furnace has been utilized to obtain our target ingots. The temperature of the electric oven was increased gradually with the rate of 50 K/h until reaching to 1373 K. The sealed silica tube with its enclosed composition was maintained at this degree for 24 h within the oven. Then, the furnace was turned off and the tube was kept in the furnace in order to cool down to room temperature. Then the silica tube was carefully broken to obtain the $CuGaGeSe_4$ ingot for its use in preparing film samples.

High-quality $CuGaGeSe_4$ thin films were successfully fabricated using the electron beam deposition (UNIVEX 450-LEYBOLD, Germany). This vacuum deposition process has two major advantages. Since the electron beam is only focused on the source material in the crucible, the latter can receive a large quantity of energy. Hence higher deposition rates for the film with greater adhesion to the substrate can be obtained. There is also a lower degree of contamination from the crucible, which can be disposed of by heating the crucible before depositing the film samples. The vacuum inside the evaporation bell jar was adjusted to be 5×10^{-5} m bar. The accelerating voltage was adjusted at 6 kV and the electron beam current was fixed at 10 mA during the deposition. Moreover, a quartz thickness monitor (Edward's FTM5) has been utilized to monitor the thickness and deposition rate of the present $CuGaGeSe_4$ films. Four film samples of different thicknesses have been physically deposited on well pre-cleaned glass substrate, the film thicknesses were 250 nm, 320 nm, 389 nm and 445 nm.

The structural properties of the $CuGaGeSe_4$ films were examined via an X-ray diffraction technique kind (X'Pert) with CuK_α radiation. Moreover, the compositional elemental percentages and the surface morphology of CuGaGeSe4 thin films have been scanned and examined by the Quanta field emission scanning electron microscope, FE-SEM of the model (FeG-250). The applied accelerating voltage was 20 kV for all obtained micrographs at different magnification powers. All measurements were made at room temperature.

The optical parameters and properties were computed and discussed via measuring the transmittance, T and reflectance, R spectra of $CuGaGeSe_4$ thin films employing a double beam spectrophotometer JASCO, Japan) of the model (SP, V-570). Using T and R measurements, the authors could obtain the absorbance, absorption coefficient, skin depth, the refractive index and its dispersion energies and parameters, in addition many other optical parameters. All optical studies were carried out at room temperature. The error in setting the optical parameters does not exceed $\pm 1\%$ at the latest.

3 Results and discussions

3.1 Structural analysis

The structural features of the $CuGaGeSe_4$ thin films have been examined via the X-Ray diffractograms, the scanning electron microscope and the energy-dispersive X-ray spectroscopy scanning. Figure 1a depicts the X-ray diffraction (XRD) of the films under

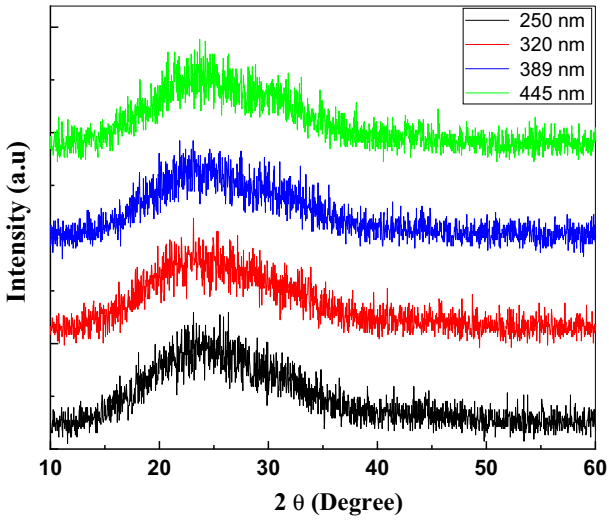

Fig. 1 X-ray diffraction patterns of the $CuGaGeSe_4$ thin films at different thicknesses, as shown, the film samples have the amorphous structure

investigation. The absence of any sharp peaks in the diffractograms has been taken as evidence for the amorphous nature of the as-prepared $CuGaGeSe_4$ thin films. The absence of the polycrystalline nature in the prepared films could be attributed to the higher energy of the electron beam of the deposition technique and owing to the short deposition time of film samples. This enhances the presence of short-range order arrangement in the prepared films.

The field emission scanning electron microscope, FE-SEM investigations of the deposited $CuGaGeSe_4$ thin films was depicted in Fig. 2. A homogeneous surface and free crack samples were obtained for the $CuGaGeSe_4$ thin films. The EDAX pattern of the $CuGaGeSe_4$ thin film with a thickness of 445 nm was depicted in Fig. 3. This pattern displays a stoichiometric composition for this investigated film (of thickness 445 nm). The micrograph confirms also the presence of the Cu, Ga, Ge, and Se peaks at their energy positions and with atomic ratios almost 1:1:1:4, respectively. The sample scanning was performed at several different places along the film surface and it was found that the values of EDAX were very close to each other. The error in the elemental percentages of any film sample was less than $\pm 1.0\%$.

3.2 Linear optical parameters

3.2.1 Transmittance and reflectance spectra

The variation of the transmittance (T) and reflectance (R) with the wavelength λ, for the deposited amorphous $CuGaGeSe_4$ thin films, were depicted in Fig. 4a, b. The analysis of these figures displayed that the transmittance of the $CuGaGeSe_4$ thin films reduced with increasing thickness of the $CuGaGeSe_4$ films owing to the increase of thin film's absorbance. On the contrary, the reflectance spectra have an opposite behaviour of the transmittance. Also, it can see that the sum of both T and R is usually less than the unity, which confirms the good optical quality of film samples. Furthermore, the absorption edge of samples was shifted towards the higher wavelengths, owing to the approach of the sample

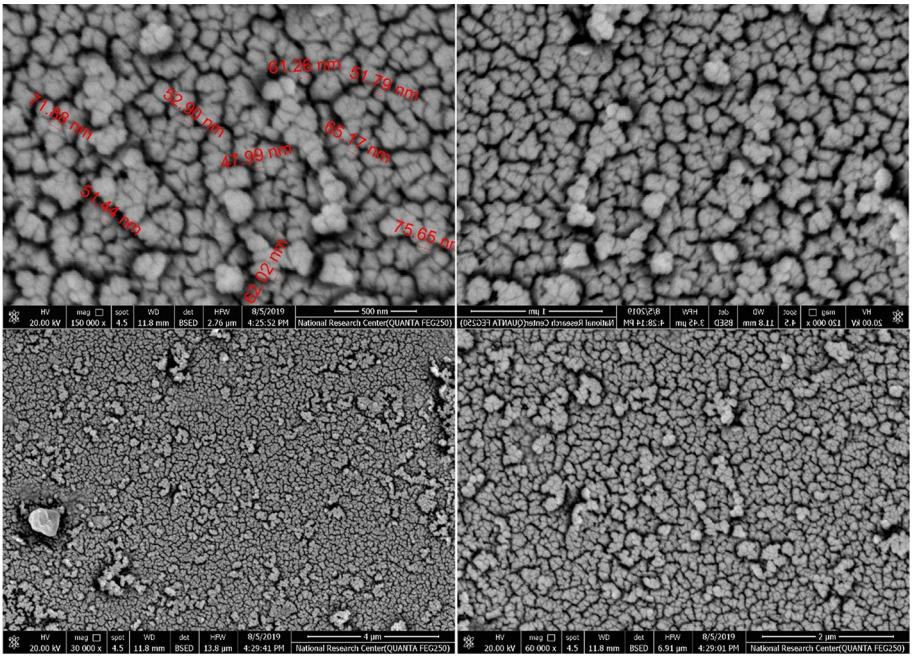

Fig. 2 The FE-SEM micrographs of the $CuGaGeSe_4$ thin films at different magnification powers, as depicted, the ternary CuGaGeSe4 thin-film samples have a homogeneous surface and free crack samples

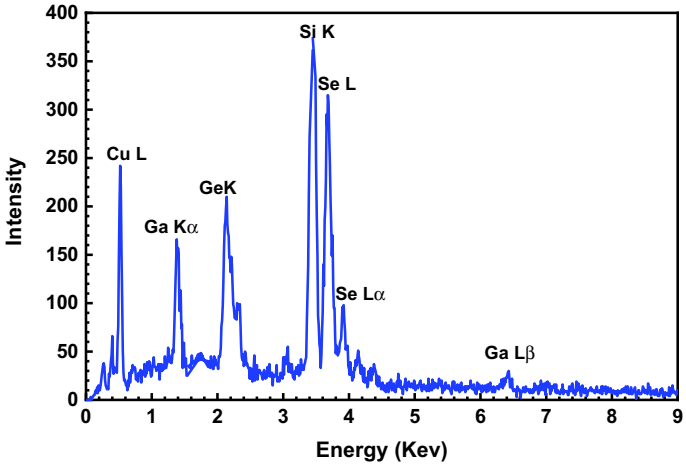

Fig. 3 The EDAX spectra of the CuGaGeSe4 thin film of the thickness 445 nm as a representative example, it displays a stoichiometric composition for this investigated film. The micrograph affirms the presence of Cu, Ga, Ge, and Se peaks with the atomic ratios 1:1:1:4, respectively

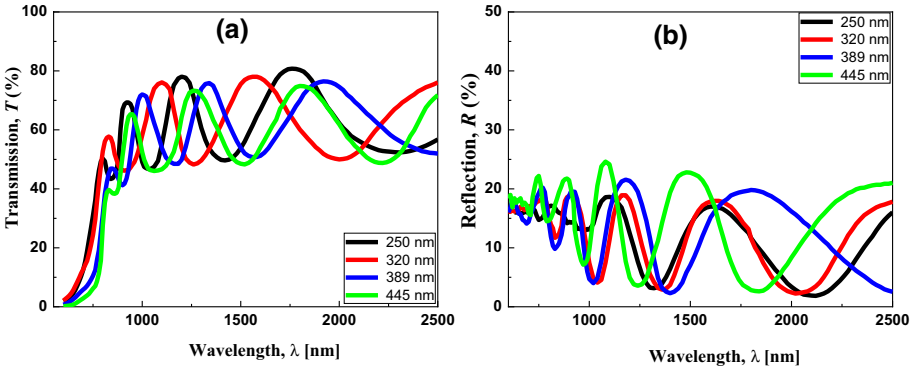

Fig. 4 The spectra of (**a**) The transmittance and (**b**) The reflectance of $CuGaGeSe_4$ films of different thicknesses as functions of the incident photon wavelength

from the bulk behaviour as the thickness increases (Hassanien and Akl 2020; Hassanien et al. 2020a, b).

3.2.2 Absorption coefficient, skin depth and energy gap evaluation

In this work, the absorption coefficient, α of the amorphous CuGaGeSe4 films with various thicknesses were evaluated employing the following equation (El-Bana et al. 2017; Hassanien and Akl 2016; Sawaby et al. 2010):

$$\alpha = \frac{1}{d} \ln \left[\frac{(1-R)^2}{2T} + \left(\frac{(1-R)^4}{4T^2} + R^2 \right)^{1/2} \right] \tag{1}$$

Here d is the film thickness.

Figure 5a demonstrated the variation of the absorption coefficient, α with the wavelength for the $CuGaGeSe_4$ thin films. This figure depicts that the absorption coefficient values increase with increasing the thickness of films. The absorption coefficient of

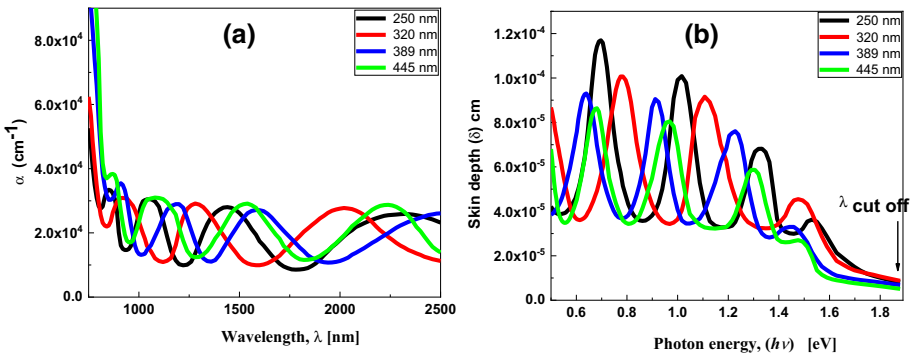

Fig. 5 **a** The absorption coefficient (α) as a function of wavelength, and **b** the skin depth (δ) versus the photon energy ($h\nu$), of $CuGaGeSe_4$ thin films at different film thicknesses

$CuGaGeSe_4$ films have high values in the range of 10^4 cm^{-1}, as the other chalcogenide film samples (Hassanien and Akl 2016).

On the other hand, the skin depth δ of the $CuGaGeSe_4$ thin films deposited at a various thicknesses (250 nm, 320 nm, 389 nm and 445 nm) has been computed via the following formula (Hassanien and Sharma 2019, 2020):

$$\delta = \frac{1}{\alpha} \tag{2}$$

The skin depth δ variation with the photon energy of the $CuGaGeSe_4$ films was depicted in Fig. 5b. It is showed from this curve that the skin depth of the $CuGaGeSe_4$ thin films was decreased with increasing the photon energy until it arrived to a certain value, which is the cut-off wavelength. The value of the cut-off energy, $E_{cut\text{-}off}$ for these amorphous $CuGaGeSe_4$ films was about 1.88 eV, which is corresponding to a cut-off wavelength, $\lambda_{cut\text{-}off}$ about 660 nm. Furthermore, the skin depth of the $CuGaGeSe_4$ films is found to decrease with increment of the film thickness.

According to the Tauc's relation, the bandgap energy of the $CuGaGeSe_4$ thin films was computed by (Tauc et al. 1966; Yahia et al. 2019):

$$\alpha h\nu = A\left(h\nu - E_g\right)^p \tag{3}$$

Here A is a some constant and p shows the optical transition process' type and it equals 1/2 and 2 for a direct allowed and indirect allowed optical transitions, correspondingly. In the presented work the proper fit was found, for the amorphous $CuGaGeSe_4$ films, $p = 2$ which implies the state of allowed indirect transition for the $CuGaGeSe_4$ thin films. This selection ($p = 2$) was obtained after many trials and plotting the different Tauc's Plots, the authors found that the longest straight line is obtained as $p = 2$, which indicates to the allowed indirect transition. This result is in good agreement for Mott and Davis Model, who suggested that the probable electronic transition for the nanocrystalline samples is the allowed indirect transition (Mott and Davis 1979; Hassanien and Akl 2018a, b). Figure 6 displays the plot of $(\alpha h\nu)^{1/2}$ versus the photon energy ($h\nu$) for the $CuGaGeSe_4$ thin films. From this plot, anyone can evaluate the optical energy gap value from the intercept of the extrapolation of the obtained straight line with the x-axis. Table 1 displayed the indirect E_g-values of the amorphous $CuGaGeSe_4$ films which decreased from 1.43 to 1.29 eV by increasing the film thickness from 250 nm to 445 nm. This behaviour could be related to the increase in structural defects that form localized states in the gap and then it decreases the film band gaps. In addition, lone-pair electrons of Se atoms form localized states at the top of the valence band tail and at the bottom of the conduction band. These formed localized states lead to shrinking of the forbidden band-gap and to cause a broadening of the tail and hence decreases the bandgap width (Hameed et al. 2019; Hassanien and Akl 2015).

3.2.3 Refractive and absorption indices

According to Kramer's–Kroning formula, the refractive index (n) of the $CuGaGeSe_4$ films was computed via this formula (Hassanien and Sharma 2020; Jebathew et al. 2019):

$$n = \frac{1+R}{1-R} + \left(\frac{4R}{(1-R)^2} - k^2\right)^{1/2} \tag{4}$$

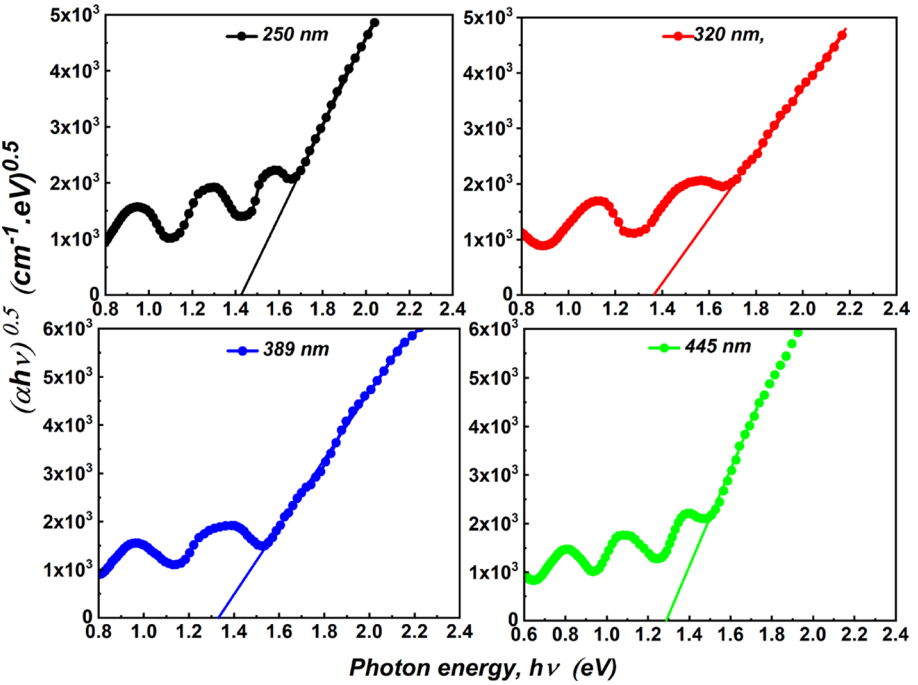

Fig. 6 The plot of $(\alpha h\nu)^{1/2}$ versus the photon energy $(h\nu)$ of the $CuGaGeSe_4$ thin films at different thicknesses, to get the indirect optical energy-gap values

Table 1 The values of the energy gap using Tauc's plots, $(E_g)^{Tuac}$, the dispersion energy, E_d, the oscillator energy, E_o, the energy gap using single oscillator model, $(E_g)^{WDD}$, Static refractive index, n_o, the static dielectric constant ε_s, and the oscillator strength, f of the quaternary $CuGaGeSe_4$ thin films, the error values of estimated values do not exceed the range of $\pm 1\%$

Film thickness (nm)	$(E_g)^{Tuac}$ (eV)	E_d (eV)	E_o (eV)	$(E_g)^{WDD}$ (eV)	n_o	ε_s	f (eV)^2
250	1.43	7.94	2.89	1.445	1.93	3.74	22.98
320	1.36	8.72	2.68	1.340	2.06	4.24	23.41
389	1.33	9.48	2.55	1.275	2.17	4.71	24.17
445	1.29	10.36	2.43	1.215	2.29	5.26	25.18

The spectral variations of the refractive index (n) with wavelength for the $CuGaGeSe_4$ films deposited at different film thickness was depicted in Fig. 7a. The analysis of this curve shows that the *n-values* of the $CuGaGeSe_4$ films were increased with increasing the film thickness. This behaviour shows a close agreement with the contribution of the electronic transition in the $CuGaGeSe_4$ thin films.

On the other hand, the absorption of light waves in the medium and the optical dielectric parameters depends mainly on a very important optical absorbing parameter, which is the absorption index, k. This index (k) can be evaluated for the $CuGaGeSe_4$ films from the following relation (Kayani et al. 2019; El Radaf et al. 2018a, b):

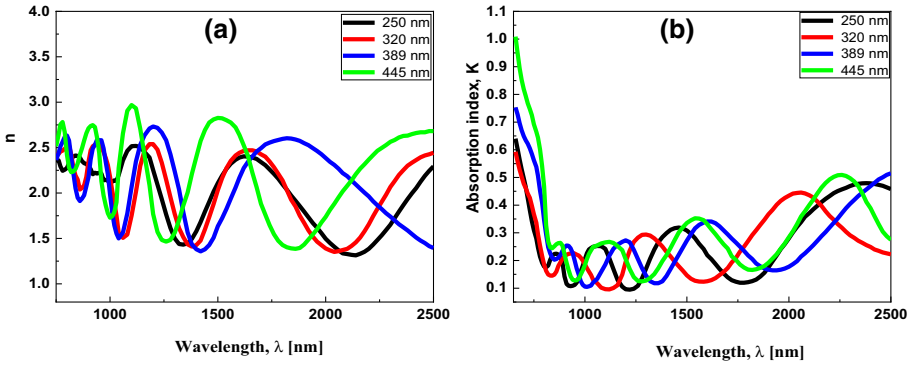

Fig. 7 **a** The refractive index and **b** the absorption index, as functions of the photon wavelength of the $CuGaGeSe_4$ thin films at different thicknesses

$$K = \frac{\alpha\lambda}{4\pi} \tag{5}$$

The spectral variation of the absorption index or the extinction coefficient (k) with the wavelength λ for the $CuGaGeSe_4$ films of different film thicknesses was displayed in Fig. 7b. It can be observed from this plot that all the curves exhibit the same trend, where the absorption index (k) increases with increasing the film thickness.

3.2.4 Dispersion energies and parameters

The dispersion energies and parameters of the $CuGaGeSe_4$ thin films have a great role in identifying the materials used in optoelectronic applications. Therefore, the dispersion parameters of the $CuGaGeSe_4$ thin films have been computed using the Wemple–DiDomenico formulas (Wemple 1973; Wemple and DiDomenico Jr 1971):

$$n^2 = 1 + \frac{E_o E_d}{E_o^2 - (h\upsilon)^2} \tag{6}$$

Here E_d represents the dispersion energy, and E_o is the single oscillator energy and n denotes the refractive index. The values of E_o and E_d for the $CuGaGeSe_4$ films were calculated according to Eq. (6) and by plotting a graph between the $(n^2-1)^{-1}$ versus the $(\hbar\upsilon)^2$ as illustrated in Fig. 8a. The graph yields a straight line its slope and intercept equivalent $(E_o E_d)^{-1}$ and (E_o/E_d) respectively.

The dependences of E_o and E_d on the thickness of the $CuGaGeSe_4$ thin films were presented in Fig. 8b. It is observed from the plot that the dispersion energy E_d raised with raising the film thickness while the oscillator energy E_o exhibits a reverse manner to E_d. Moreover the static dielectric constant ε_s, the static refractive index n_o and the oscillator strength f of the $CuGaGeSe_4$ films were evaluated according to the presented relations (Aly 2010; Hassanien 2016; Mohamed et al. 2019; Sharma and Katyal 2008):

$$f = E_o E_d \tag{7}$$

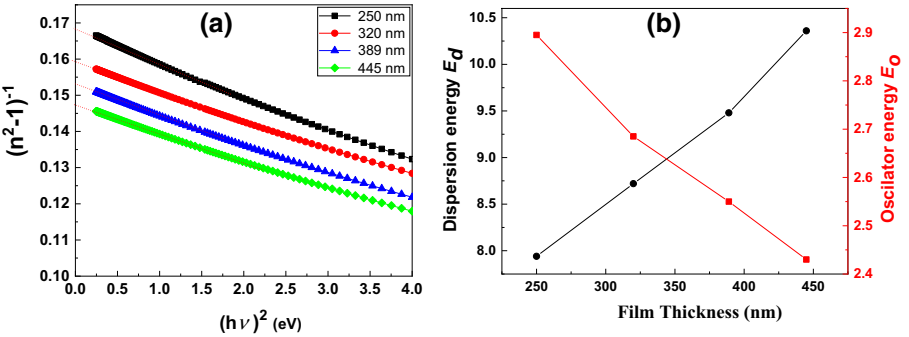

Fig. 8 **a** The dependence of $(n^2-1)^{-1}$ on $(h\nu)^2$ and **b** The variation of dispersion energies (E_o and E_d) with the film thickness, of the $CuGaGeSe_4$ thin films at different thicknesses

$$n_o = \sqrt{1 + \frac{E_d}{E_o}} \tag{8}$$

$$\varepsilon_s = n_o^2 \tag{9}$$

Table 1 displayed the determined values of the static dielectric constant ε_s, the static refractive index n_o and the oscillator strength f of the amorphous $CuGaGeSe_4$ thin films. It is observed that, increasing the film thickness leads to increase the values of the dispersion energy, E_d, the static index of refraction, n_o, the static dielectric constant, ε_s, and the dielectric strength, f of these novel chalcogenide $CuGaGeSe_4$ thin-film samples.

3.3 Optoelectrical parameters

3.3.1 Optical dielectric constants

According to the n and k calculations, the real and imaginary part of the dielectric constants of the $CuGaGeSe_4$ films were computed by these simple formulas (El-Nahass and Farag 2012; El Radaf and Abdelhameed 2018):

$$\varepsilon_1 = n^2 - k^2 \tag{10}$$

$$\varepsilon_2 = 2nk \tag{11}$$

Here ε_1 and ε_2 present the real and the imaginary part of the dielectric constant. Figure 9a, b depicts that the value of ε_1 and ε_2 increase with increasing the film thickness. These good obtained results and the performance of the dielectric parameters reveals the good optical response of the amorphous CuGaGeSe4 thin films.

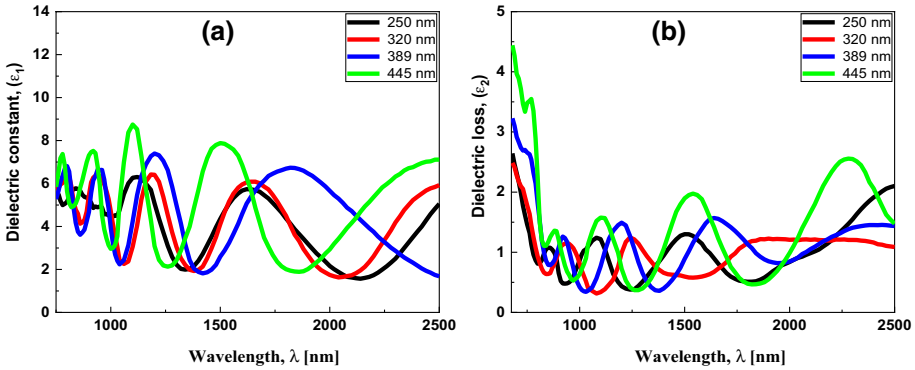

Fig. 9 The variation of the **a** Real dielectric constant and **b** Imaginary dielectric constant, as functions of the wavelength of the incident photon for the $CuGaGeSe_4$ thin films

3.3.2 Optical carrier concentration and relaxation time

In this study, both the charge carrier concentration to effective mass ratio (N_{opt}/m^*), and the lattice dielectric constant ε_L, of the $CuGaGeSe_4$ films can be evaluated via the relation (Fouad

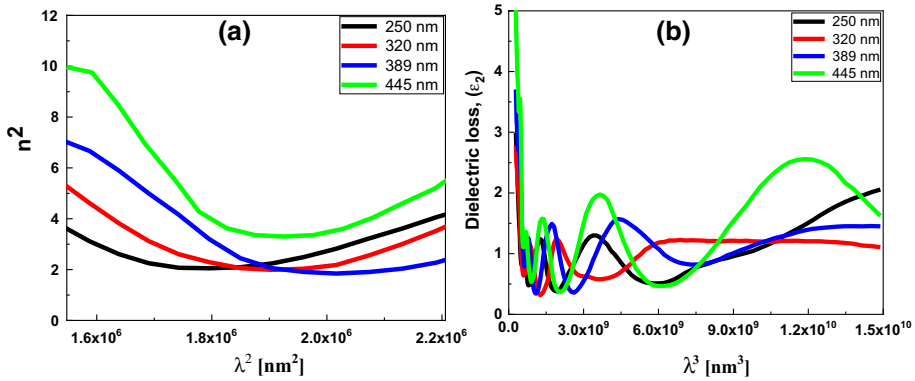

Fig. 10 **a** The variation of (n^2) with (λ^2) and (**b**) The dependence of imaginary dielectric constant (ε_2) on the (λ^3), of the CuGaGeSe4 thin films at different thicknesses

Table 2 The lattice dielectric constant, ε_L, the ratio of the charge carrier concentrations to the effective mass (N_{opt}/m^*), time constant, τ, optical mobility, μ_{opt}, optical resistivity, ρ_{opt}, third order susceptibility, $\chi^{(3)}$, and nonlinear refractive index, n_2 of the $CuGaGeSe_4$ thin films of different thicknesses (the error values of estimated values do not exceed the range of ± 1%)

Film thickness (nm)	ε_L	N_{opt}/m^* ($\times 10^{42}$) (g^{-1} cm^{-3})	τ ($\times 10^{-25}$) s	μ_{opt} ($\times 10^{-6}$) (C s/kg)	ρ_{opt} ($\times 10^{57}$) ($\frac{kg\ m^3}{C\ s}$)	$\chi^{(3)} \times 10^{-12}$ (esu)	$n_2 \times 10^{-11}$ (esu)
250	3.72	49.76	9.27	4.47	1.39	0.38	0.75
320	4.21	50.97	8.175	4.86	1.54	0.75	1.38
389	4.65	53.61	7.14	5.69	1.90	1.31	2.26
445	5.04	55.01	6.72	6.98	2.39	2.25	3.71

et al. 2006; El Radaf 2019):

$$n^2 = \varepsilon_L - \left(\frac{e^2}{4\pi^2 c^2 \varepsilon_0}\right)\left(\frac{N_{opt}}{m^*}\right)\lambda^2 \tag{12}$$

Here e is the electronic charge, c represents the speed of light, while ε_o represents the electric permittivity of free space. Figure 10a implies the reliance of n^2 on λ^2 for the $CuGaGeSe_4$ films. The values obtained for both (N_{opt}/m^*), ε_L are listed in Table 2. It is observed that the ratio N_{opt}/m^* raises with enlarging the film thickness. This indicates that the expansion in film thickness is associated with an increase in the charge carrier concentration. This could be attributed to the increase in the lone-pair electrons of Se atom in the film. On the other hand, the values of ε_L increases with increasing the film thickness. This trend could be attributed to the possibility of achieving a degree of ordering in the $CuGaGeSe_4$ films which enhance atoms arrangements in the film as contrasted to other investigated films. Hence the ε_L value increases in this film.

Furthermore, the relaxation time, τ, of the $CuGaGeSe_4$ films can be determined by utilizing the following formula (Ali et al. 2018; Elsaeedy 2019):

$$\varepsilon_2 = \frac{1}{4\pi^3 \varepsilon_0}\left(\frac{e^2}{c^3}\right)\left(\frac{N_{opt}}{m^*}\right)\left(\frac{1}{\tau}\right)\lambda^3 \tag{13}$$

The dependence of imaginary dielectric constant ε_2 on the alteration in λ^3 or the $CuGaGeSe_4$ films is presented in Fig. 10b and we can evaluate the relaxation times, τ, of the $CuGaGeSe_4$ thin films from the slope of this figure. In addition, the values of relaxation times, τ, for the $CuGaGeSe_4$ thin films found to decrease with raising the film thickness.

3.3.3 Optical mobility and optical resistivity

In this work, the optical resistivity ρ_{opt} and the optical mobility μ_{opt} of the $CuGaGeSe_4$ films have been computed via the expressions (Hamrouni et al. 2018; Sharma et al. 2016):

$$\rho_{opt} = \frac{1}{e}\mu_{opt} N_{opt} \tag{14}$$

$$\mu_{opt} = \frac{e\tau}{m^*} \tag{15}$$

The computed values of both the optical resistivity ρ_{opt} and the optical mobility μ_{opt} are recorded in Table 2 for the present amorphous $CuGaGeSe_4$ films deposited at various thicknesses. It is observed that the value of both the μ_{opt} and ρ_{opt} increase with increment of the film thickness. These results are in good consistency with the other previously published works (Shkir et al. 2019a, b).

3.3.4 Optical and electrical conductivity

The optical and electrical conductivities of the $CuGaGeSe_4$ thin films were computed via the following expressions (Darwish et al. 2019; AlKhalifah et al. 2020):

$$\sigma_{opt} = \frac{\alpha n c}{4\pi} \tag{16}$$

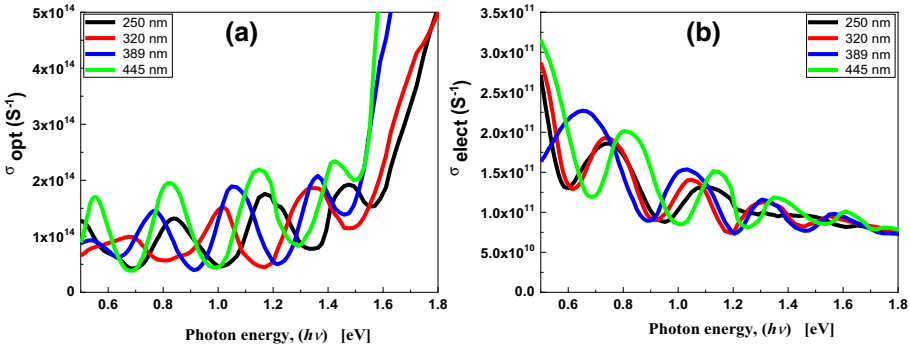

Fig. 11 **a** The dependence of the optical conductivity and **b** The electrical conductivity as functions of the photon energy for the $CuGaGeSe_4$ thin films

$$\sigma_e = \frac{2\lambda\sigma_{opt}}{\alpha} \tag{17}$$

Here σ_{opt} denotes the optical conductivity, c represents the speed of light, σ_e denotes the electrical conductivity, α denotes the absorption coefficient and n is the refractive index.

Figure 11a depicts the variation of the optical conductivity with the photon energy for the present amorphous $CuGaGeSe_4$ films. It can observe from this figure that the optical conductivity values increase with increasing the film thickness. This is due to the increasing of the charge carriers (see Table 2). Moreover, the optical conductivity increases also as increasing the incident photon energy. This trend could be interpreted as a result of increasing the excitation process of the electronic charges by increasing the incident photon energy. Figure 11b illustrates the variation of the electrical conductivity as function of the photon energy for the $CuGaGeSe_4$ films. It can be seen from this curve that, the electrical conductivity values of the $CuGaGeSe_4$ films increase also with increasing the film thickness; while they decrease as increasing the incident photon energy.

3.4 Nonlinear optical characterization

The investigation of the nonlinear characteristics of any semiconducting material is very important, where the knowledge of theses information paves the way for detecting the possibility of exploiting studied materials in various applications such as high capacity communication systems, optical circuits, and photonic applications. In this study, the third-order nonlinear optical susceptibility $\chi^{(3)}$ and the magnitudes of the nonlinear refractive index n_2 for the $CuGaGeSe_4$ films was computed by the below Miller's formulas (Alharbi et al. 2016; Darwish et al. 2017; Ganesh et al. 2017; El Radaf et al. 2019b; Shkir et al. 2019b):

$$\chi^{(3)} = B\left[\frac{n_0^2 - 1}{4\pi}\right]^4 \tag{18}$$

$$n_2 = \frac{12\pi\chi^{(3)}}{n_0} \tag{19}$$

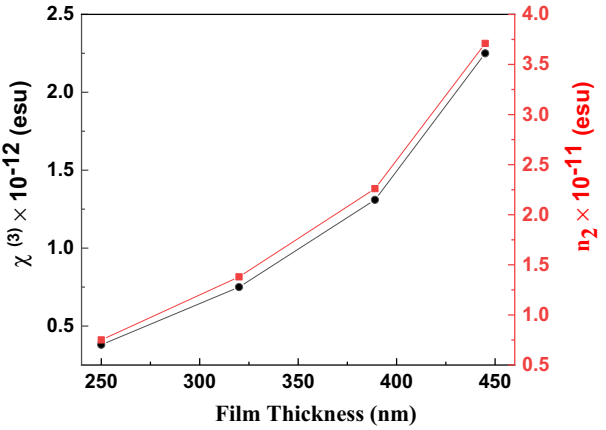

Fig. 12 The dependence of third-order nonlinear optical susceptibility ($\chi^{(3)}$) and nonlinear refractive index (n_2) on the thickness for the $CuGaGeSe_4$ thin films

where n_0 represents the value of the static refractive index and B is a constant value, equals to 1.7×10^{-10} esu (Hassanien et al. (2016). Table 2 displays the values of $\chi^{(3)}$ and n_2 of the amorphous $CuGaGeSe_4$ films of different thicknesses. Moreover, Fig. 12 depicts also that the values of $\chi^{(3)}$ and n_2 of the $CuGaGeSe_4$ films increases as increasing the film thickness.

4 Conclusions

In this work, the electron beam deposition technique was employed to synthesis good quality $CuGaGeSe_4$ thin films at different thickness. The XRD results presented that the $CuGaGeSe_4$ films have the amorphous nature. The energy dispersive X-ray spectroscopy analysis, EDAX confirmed the elemental composition percentages, where the elemental ratios were detected as 1:1:1:4, which affirm the chemical composition of the amorphous $CuGaGeSe_4$ thin films. The transmission and reflection spectra were utilized to produce and analysis the optical properties of the film samples. The optical results displayed that the skin depth and the indirect optical band gap of the $CuGaGeSe_4$ films were found to decrease with increase the film thickness, while the absorption coefficient has the opposite behaviour.

The refractive index dispersion energies and parameters of the $CuGaGeSe_4$ films were computed and discussed. It was found that increasing the film thickness of the amorphous $CuGaGeSe_4$ thin-film samples leads to increase the dispersion energy, static refractive index, static dielectric constant, oscillator strength. On the contrary, the oscillator energy, the relaxation time and the energy gap using single oscillator model, $(E_g)^{WDD}$ were decreased. Moreover, the optical conductivity and the non-linear optical parameters of the $CuGaGeSe_4$ thin films were increased with the film thickness. These results are in good matching with the results previously obtained, which confirm on the good quality of the film samples.

These good optical findings strongly support the use of these films in many potential optical applications, especially in solar cells as a good absorber layer for thin-film solar cells. Therefore, these CuGaGeSe4 thin films can be used as a substitute for the films of "CuInGaSe2", since their optical properties strongly qualify them to be used, in addition to the abundance of their ore materials and lower costs of their preparation.

Funding This research was not funded by any authority, entity or individual other than the authors themselves. The authors have born all the costs of the work

Compliance with ethical standards

Conflict of interest The authors declare that they have no conflict of interest.

References

Aldakov, D., Lefrançois, A., Reiss, P.: Ternary and quaternary metal chalcogenide nanocrystals: synthesis, properties and applications. J. Mater. Chem. C **1**, 3756–3776 (2013)

Alharbi, S.R., Darwish, A.A.A., Al Garni, S.E., ElSaeedy, H.I., El-Rahman, K.F.A.: Influence of thickness and annealing on linear and nonlinear optical properties of manganese (III) chloride tetraphenyl porphine (MnTPPCl) organic thin films. Infrared Phys. Technol. **78**, 77–83 (2016)

Ali, H.A.M., El-Nahass, M.M., El-Zaidia, E.F.M.: Optical and dispersion properties of thermally deposited phenol red thin films. Opt. Laser Technol. **107**, 402–407 (2018). https://doi.org/10.1016/j.optlastec.2018.06.001

AlKhalifah, M.S., El Radaf, I.M., El-Bana, M.S.: New window layer of Cu2CdSn3S8 for thin film solar cells. J. Alloys Compd. **813**, 152169 (2020). https://doi.org/10.1016/j.jallcom.2019.152169

Aly, K.A.: Optical band gap and refractive index dispersion parameters of As x Se 70 Te $30-x$ ($0 \le x \le 30$ at.%) amorphous films. Appl. Phys. A **99**, 913–919 (2010)

Benchikri, M., Zaberca, O., El Ouatib, R., Durand, B., Oftinger, F., Balocchi, A., Chane-Ching, J.-Y.: A high temperature route to the formation of highly pure quaternary chalcogenide particles. Mater. Lett. **68**, 340–343 (2012)

Chen, S., Gong, X.G., Walsh, A., Wei, S.-H.: Electronic structure and stability of quaternary chalcogenide semiconductors derived from cation cross-substitution of II-VI and I-III-VI 2 compounds. Phys. Rev. B. **79**, 165211 (2009)

Chen, S., Walsh, A., Luo, Y., Yang, J.-H., Gong, X.G., Wei, S.-H.: Wurtzite-derived polytypes of kesterite and stannite quaternary chalcogenide semiconductors. Phys. Rev. B **82**, 195203 (2010)

Darwish, A.A.A., Rashad, M., Bekheet, A.E., El-Nahass, M.M.: Linear and nonlinear optical properties of GeSe2-xSnx ($0 \le x \le 0.8$) thin films for optoelectronic applications. J. Alloys Compd. **709**, 640–645 (2017)

Darwish, A.A.A., Qashou, S.I., Rashad, M.: Structural, surface topography and optical investigations of nanostructure films of copper(II) 2,9,16,23-teter-tert-butyl-29H,31H-phthalocyanine controlled at thermal effect. Appl. Phys. A Mater. Sci. Process. (2019). https://doi.org/10.1007/s00339-019-2559-z

El Radaf, I.M.: Structural, optical, optoelectrical and photovoltaic properties of the thermally evaporated Sb_2Se_3 thin films. Appl. Phys. A **125**, 832 (2019)

El Radaf, I.M., Abdelhameed, R.M.: Surprising performance of graphene oxide/tin dioxide composite thin films. J. Alloys Compd. **765**, 1174–1183 (2018)

El Radaf, I.M., Fouad, S.S., Ismail, A.M., Sakr, G.B.: Influence of spray time on the optical and electrical properties of $CoNi_2S_4$ thin films. Mater. Res. Express **5**, 46406 (2018a)

El Radaf, I.M., Hamid, T.A., Yahia, I.S.: Synthesis and characterization of F-doped CdS thin films by spray pyrolysis for photovoltaic applications. Mater. Res. Express (2018b). https://doi.org/10.1088/2053-1591/aaca7b

El Radaf, I.M., Elsaeedy, H.I., Yakout, H.A., El Sayed, M.T.: Junction Parameters and Electrical Characterization of the Al/n-Si/Cu_2CoSnS_4/Au Heterojunction. J. Electron. Mater. (2019a). https://doi.org/10.1007/s11664-019-07445-7

El Radaf, I.M., Hameed, T.A., El Komy, G.M., Dahy, T.M.: Synthesis, structural, linear and nonlinear optical properties of chromium doped SnO_2 thin films. Ceram. Int. **45**, 3072–3080 (2019b). https://doi.org/10.1016/j.ceramint.2018.10.189

El Radaf, I.M., Al-Zahrani, H.Y.S., Hassanien, A.S.: Novel synthesis, structural, linear and nonlinear optical properties of p-type kesterite nanosized Cu_2MnGeS_4 thin films. J. Mater. Sci. Mater. Electron. **31**, 8336–8348 (2020). https://doi.org/10.1007/s10854-020-03369-9

El-Bana, M.S., El Radaf, I.M., Fouad, S.S., Sakr, G.B.: Structural and optoelectrical properties of nanostructured $LiNiO_2$ thin films grown by spray pyrolysis technique. J. Alloys Compd. **705**, 333–339 (2017)

El-Nahass, M.M., Farag, A.A.M.: Structural, optical and dispersion characteristics of nanocrystalline GaN films prepared by MOVPE. Opt. Laser Technol. **44**, 497–503 (2012). https://doi.org/10.1016/j.optlastec.2011.08.021

Elsaeedy, H.I.: Growth, structure, optical and optoelectrical characterizations of the Cu_2 $NiSnS_4$ thin films synthesized by spray pyrolysis technique. J. Mater. Sci. Mater. Electron. **30**, 12545–12554 (2019)

Fouad, S.S., El-Shazly, E.A.A., Balboul, M.R., Fayek, S.A., El-Bana, M.S.: Optical parameter studies of thermally evaporated As–Se–Sn glassy system. J. Mater. Sci. Mater. Electron. **17**, 193–198 (2006)

Fouad, S.S., El Radaf, I.M., Sharma, P., El-Bana, M.S.: Multifunctional CZTS thin films: structural, optoelectrical, electrical and photovoltaic properties. J. Alloys Compd. **757**, 124–133 (2018)

Ganesh, V., Yahia, I.S., AlFaify, S., Shkir, M.: Sn-doped ZnO nanocrystalline thin films with enhanced linear and nonlinear optical properties for optoelectronic applications. J. Phys. Chem. Solids **100**, 115–125 (2017)

Hameed, T.A., El Radaf, I.M., Elsayed-Ali, H.E.: Characterization of $CuInGeSe_4$ thin films and Al/n–Si/p–CuInGeSe4/Au heterojunction device. J. Mater. Sci. Mater. Electron. **29**, 12584–12594 (2018). https://doi.org/10.1007/s10854-018-9375-7

Hameed, T.A., Wassel, A.R., El Radaf, I.M.: Investigating the effect of thickness on the structural, morphological, optical and electrical properties of $AgBiSe_2$ thin films. J. Alloys Compd. **805**, 1–11 (2019). https://doi.org/10.1016/j.jallcom.2019.07.041

Hamrouni, S., AlKhalifah, M.S., El-Bana, M.S., Zobaidi, S.K., Belgacem, S.: Deposition and characterization of spin-coated n-type ZnO thin film for potential window layer of solar cell. Appl. Phys. A **124**, 555 (2018)

Hassanien, A.S.: Studies on dielectric properties, opto-electrical parameters and electronic polarizability of thermally evaporated amorphous $Cd_{50}S_{50-x}Se_x$ thin films. J. Alloys Compd. **671**, 566–578 (2016)

Hassanien, A.S., Akl, A.A.: Influence of composition on optical and dispersion parameters of thermally evaporated non-crystalline $Cd_{50}S_{50-x}Se_x$ thin films. J. Alloys Compd. **648**, 280–290 (2015)

Hassanien, A.S., Akl, A.A.: Effects of Se on optical and electrical properties of chalcogenide CdSSe thin films. Superlattices Microstruct. **89**, 153–169 (2016)

Hassanien, A.S., Akl, A.A.: Influence of thermal and compositional variations on conduction mechanisms and localized state density of amorphous $Cd_{50}S_{50-x}Se_x$ thin films. J. Non-Cryst. Solids **487**, 28–36 (2018a). https://doi.org/10.1016/j.jnoncrysol.2018.02.018

Hassanien, A.S., Akl, A.A.: Optical characteristics of iron oxide thin films prepared by spray pyrolysis technique at different substrate temperatures. Appl. Phys. A **124**, 752 (2018b). https://doi.org/10.1007/s00339-018-2180-6

Hassanien, A.S., Akl, A.A.: X-ray studies: CO_2 pulsed laser annealing effects on the crystallographic properties, microstructures and crystal defects of vacuum-deposited nanocrystalline ZnSe thin films. CrystEngComm **20**(44), 7120–7129 (2018c)

Hassanien, A.S., Akl, A.A.: Optical characterizations and refractive index dispersion parameters of annealed TiO_2 thin films synthesized by RF-sputtering technique at different flow rates of the reactive oxygen gas. Physica B **576**, 411718 (2020). https://doi.org/10.1016/j.physb.2019.411718

Hassanien, A.S., El Radaf, I.M.: Optical characterizations of quaternary Cu_2MnSnS_4 thin films: novel synthesis process of film samples by spray pyrolysis technique. Phys. B **585**, 412110 (2020). https://doi.org/10.1016/j.physb.2020.412110

Hassanien, A.S., Sharma, I.: Band-gap engineering, conduction and valence band positions of thermally evaporated amorphous Ge_{15-x} Sb_x Se_{50} Te_{35} thin films: influences of Sb upon some optical characterizations and physical parameters. J. Alloys Compd. **798**, 750–763 (2019). https://doi.org/10.1016/j.jallcom.2019.05.252

Hassanien, A.S., Sharma, I.: Optical properties of quaternary a-$Ge_{15-x}Sb_x$ Se_{50} Te_{35} thermally evaporated thin-films: refractive index dispersion and single oscillator parameters. Optik **200**, 163415 (2020). https://doi.org/10.1016/j.ijleo.2019.163415

Hassanien, A.S., Aly, K.A., Akl, A.A.: Optical properties of thermally evaporated ZnSe thin films annealed at different pulsed leaser powers. J. Alloys Compd. **685**, 733–742 (2016)

Hassanien, A.S., Sharma, I., Akl, A.A.: Physical and optical properties of $Ge_{15-x}Sb_xSe_{50}Te_{35}$ bulk and film samples: refractive index and its association with electronic polarizability of thermally evaporated a-Ge–Sb–Se–Te thin-films. J. Non-Cryst. Solids **531**, 119853 (2020a). https://doi.org/10.1016/j.jnoncrysol.2019.119853

Hassanien, A.S., Neffati, R., Aly, K.A.: Impact of Cd-addition upon optical properties and dispersion parameters of thermally evaporated $Cd_xZn_{1-x}Se$ films: discussions on bandgap engineering, conduction and valence band positions. Optik **212**, 164681 (2020b). https://doi.org/10.1016/j.ijleo.2020.164681

Jebathew, A.J., Karunakaran, M., Kumar, K.D.A., Valanarasu, S., Ganesh, V., Shkir, M., Yahia, I.S., Zahran, H.Y., Kathalingam, A.: An effect of Gd3 + doping on core properties of ZnS thin films prepared by nebulizer spray pyrolysis (NSP) method. Phys. B Condens. Matter. **574**, 411674 (2019)

Kayani, Z.N., Arshad, S., Riaz, S., Naseem, S.: Investigation of structural, optical and magnetic characteristics of Co_3O_4 thin films. Appl. Phys. A Mater. Sci. Process. (2019). https://doi.org/10.1007/s00339-019-2501-4

Liu, M.-L., Huang, F.-Q., Chen, L.-D., Chen, I.-W.: A wide-band-gap p-type thermoelectric material based on quaternary chalcogenides of Cu_2 ZnSn Q 4 (Q = S, Se). Appl. Phys. Lett. **94**, 202103 (2009)
Mohamed, M., Shaaban, E.R., Abd-el Salam, M.N., Abdel-Latief, A.Y., Mahmoud, S.A., Abdel-Rahim, M.A.: Investigation of the optical and electrical parameters of As47.5Se47.5Ag5 thin films with different thicknesses for optoelectronic applications. Optik **178**, 1302–1312 (2019). https://doi.org/10.1016/j.ijleo.2018.10.103
Mott, N.F., Davis, E.A.: Electronic Processes in Non-crystalline Materials. Clarendon Press, Oxford (1979)
Ramasamy, K., Malik, M.A., O'Brien, P.: Routes to copper zinc tin sulfide Cu_2ZnSnS_4 a potential material for solar cells. Chem. Commun. (2012). https://doi.org/10.1039/c2cc30792h
Ramasamy, P., Kim, M., Ra, H.-S., Kim, J., Lee, J.-S.: Bandgap tunable colloidal Cu-based ternary and quaternary chalcogenide nanosheets via partial cation exchange. Nanoscale **8**, 7906–7913 (2016)
Sawaby, A., Selim, M.S., Marzouk, S.Y., Mostafa, M.A., Hosny, A.: Structure, optical and electrochromic properties of NiO thin films. Phys. B Condens. Matter. **405**, 3412–3420 (2010)
Schäfer, W., Nitsche, R.: Tetrahedral quaternary chalcogenides of the type Cu2-II-IV-S4 (Se4). Mater. Res. Bull. **9**, 645–654 (1974)
Schurr, R., Hölzing, A., Jost, S., Hock, R., Voß, T., Schulze, J., Kirbs, A., Ennaoui, A., Lux-Steiner, M., Weber, A., Kötschau, I., Schock, H.W.: The crystallisation of Cu_2ZnSnS_4 thin film solar cell absorbers from co-electroplated Cu–Zn–Sn precursors. Thin Solid Films (2009). https://doi.org/10.1016/j.tsf.2008.11.019
Scragg, J.J., Dale, P.J., Peter, L.M.: Synthesis and characterization of Cu_2ZnSnS_4 absorber layers by an electrodeposition-annealing route. Thin Solid Films (2009). https://doi.org/10.1016/j.tsf.2008.11.022
Sharma, P., Katyal, S.C.: Effect of tin addition on the optical parameters of thermally evaporated As–Se–Ge thin films. Mater. Chem. Phys. **112**, 892–897 (2008)
Sharma, P., El-Bana, M.S., Fouad, S.S., Sharma, V.: Effect of compositional dependence on physical and optical parameters of Te17Se83 − xBix glassy system. J. Alloys Compd. **667**, 204–210 (2016)
Shi, J.H., Li, Z.Q., Zhang, D.W., Liu, Q.Q., Sun, Z., Huang, S.M.: Fabrication of Cu (In, Ga) Se2 thin films by sputtering from a single quaternary chalcogenide target. Prog. Photovolt. Res. Appl. **19**, 160–164 (2011)
Shi, C., Shi, G., Chen, Z., Yang, P., Yao, M.: Deposition of Cu_2ZnSnS_4 thin films by vacuum thermal evaporation from single quaternary compound source. Mater. Lett. **73**, 89–91 (2012)
Shkir, M., Arif, M., Singh, A., Yahia, I.S., Algarni, H., AlFaify, S.: A facile one-step flash combustion synthesis and characterization on C doped NiO nanostructures. Mater. Sci. Semicond. Process. **100**, 106–112 (2019a). https://doi.org/10.1016/j.mssp.2019.04.038
Shkir, M., Khan, A., El-Toni, A.M., Aldalbahi, A., Yahia, I.S., AlFaify, S.: Structural, morphological, opto-nonlinear-limiting studies on Dy:pbI 2/FTO thin films derived facilely by spin coating technique for optoelectronic technology. J. Phys. Chem. Solids **130**, 189–196 (2019b). https://doi.org/10.1016/j.jpcs.2019.02.030
Tauc, J., Grigorovici, R., Vancu, A.: Optical properties and electronic structure of amorphous germanium. Phys. Status Solidi **15**, 627–637 (1966)
Wemple, S.H.: Refractive-index behavior of amorphous semiconductors and glasses. Phys. Rev. B. **7**, 3767 (1973)
Wemple, S.H., DiDomenico Jr., M.: Behavior of the electronic dielectric constant in covalent and ionic materials. Phys. Rev. B **3**, 1338 (1971)
Yahia, I.S., El Radaf, I.M., Salem, A.M., Sakr, G.B.: Chemically deposited Ni-doped CdS nanostructured thin films: optical analysis and current–voltage characteristics. J. Alloys Compd. **776**, 1056–1062 (2019)
Zamani, R.R., Ibánez, M., Luysberg, M., Garcia-Castello, N., Houben, L., Prades, J.D., Grillo, V., Dunin-Borkowski, R.E., Morante, J.R., Cabot, A.: Polarity-driven polytypic branching in Cu-based quaternary chalcogenide nanostructures. ACS Nano **8**, 2290–2301 (2014)
Ziti, A., Hartiti, B., Labrim, H., Fadili, S., Tchognia Nkuissi, H.J., Ridah, A., Tahri, M., Thevenin, P.: Effect of copper concentration on physical properties of CZTS thin films deposited by dip-coating technique. Appl. Phys. A Mater. Sci. Process. (2019). https://doi.org/10.1007/s00339-019-2513-0

Affiliations

Ahmed Saeed Hassanien[1,2] · Hatem R. Alamri[3] · I. M. El Radaf[4,5]

Ahmed Saeed Hassanien
a.s.hassanien@gmail.com; ahmed.hassanien@feng.bu.edu.eg

1 Engineering Mathematics and Physics Department, Faculty of Engineering at Shoubra - Cairo, Benha University, Benha 11629, Egypt

2 Physics Department, Faculty of Science and Humanities in Afif Governorate, Shaqra University, Afif 11921, Kingdom of Saudi Arabia

3 Physics Department, Al Jumum University College, Umm Al-Qura University, Makkah 21955, Kingdom of Saudi Arabia

4 Physics Division, Electron Microscope and Thin Films Department, National Research Centre, Dokki, Giza 12622, Egypt

5 Materials Physics and Energy Laboratory, College of Sciences and Art at ArRass, Qassim University, Ar Rass 51921, Kingdom of Saudi Arabia